Histol Histopathol (2019) 34: 1377-1385

http://www.hh.um.es

Histology and Histopathology

From Cell Biology to Tissue Engineering

HGSNAT enzyme deficiency results in accumulation of heparan sulfate in podocytes and basement membranes

Lauren Nagel[1], Regiana Oliveira[1], Alexey V. Pshezhetsky[2] and Carlos R. Morales[1]

[1]Department of Anatomy and Cell Biology, McGill University and [2]Division of Medical Genetics, Centre Hospitalière Universitaire Sainte-Justine, University of Montréal, Montréal, Quebec, Canada

Summary. Mucopolysaccharidosis III type C is a lysosomal storage disorder caused by the accumulation of heparan sulfate in lysosomes. The disorder occurs due to Heparan Acetyl-CoA: α-glucosaminide N-acetyltransferase (HGSNAT) deficiency, an enzyme which typically catalyzes the transmembrane acetylation of heparan sulfate, a basement membrane component. When the gene encoding this enzyme is mutated, it cannot perform the processing of heparan sulfate, leading to un-acetylated heparan sulfate build-up in the lysosomes of cells, causing a storage disorder. This defect has been studied primarily in brain and liver cells, but its effect on the structural integrity of the glomerulus is poorly known. The present study focuses on the effect of *Hgsnat* gene inactivation and heparan sulfate toxicity on the integrity of the renal corpuscle. This cortical structure was chosen because of its abundance of basement membranes and heparan sulfate as well as the renal corpuscle's physiological importance in glomerular filtration. Light microscopy, electron microscopy, and immunocytochemistry of genetically modified mice revealed a buildup of lysosomes in the podocytes, suggesting that these cells are responsible for the processing of glomerular basement membranes.

Key words: Heparan sulfate, Lysosome, HGSNAT, Renal corpuscle, Podocyte

Offprint requests to: Carlos R. Morales, Department of Anatomy and Cell Biology, McGill University, Montreal, Quebec, Canada. e-mail: carlos.morales@mcgill.ca

DOI: 10.14670/HH-18-131

Introduction

Mucopolysaccharidosis III type C (MPS IIIC), also known as Sanfilippo Syndrome C, is a metabolic storage disease characterized by severe neurological deterioration (Martins, et al., 2015). Hyperactivity, sleep disorders, loss of speech, hearing loss, and mental retardation are some of the frequent clinical manifestations of the disease (Valstar et al., 2008). The disorder is caused by the inability of lysosomes to properly digest a linear polysaccharide, heparan sulfate, due to a lack of a functional heparan sulfate acetyl-CoA: α-glucosaminide N-acetyl- transferase (HGSNAT) (Hrebicek et al., 2006). HGSNAT is a lysosomal membrane enzyme that catalyzes the transmembrane acetylation of the terminal glucosamine residues of heparan sulfate, a step required for its subsequent processing (Bame and Rome, 1986). Lack of heparan sulfate acetylation results in its accumulation in lysosomes (Bartsocas et al., 1979). In the brain, accumulation of heparan sulfate causes neuro-inflammation and neuronal death, leading to a full-scale neurodegenerative disease (Martins et al., 2015). Previous studies have demonstrated more than 80 different *Hgsnat* mutations; nonsense, missense, deletions, and insertions, all causing deficient enzymatic activity in the patient's cells (Feldhammer et al., 2009).

In the kidney, heparan sulfate is found primarily in basement and plasma cell membranes as well as in

Abbreviations. HGSNAT, Heparan Acetyl-CoA: α-glucosaminide N-acetyltransferase; HS, hepran sulfate; MPS IIIC, Mucopolysaccharidosis III type C

extracellular matrices (Bame, 2001). Basement membranes are particularly abundant in the renal corpuscle where they lie under the parietal layer of the Bowman's capsule and between the fenestrated endothelium of the glomerular capillaries and the pedicels of podocytes (White, 2012). Here they play an important role in glomerular filtration, the fundamental task of the kidney (Miner, 2012).

We predicted that the pathological effects of the HGSNAT deficiency would be most visible in the glomeruli of the renal corpuscles, as basement membranes are particularly thick and abundant within these structures (Bishop et al., 2007; Miner, 2012). We also hypothesized that the mesangial cells would be the most probable target for the lysosomal buildup as these cells are located between the glomerular capillaries and have been suggested to be involved in both synthesis and phagocytic removal of glomerular components (Wilson and Steward, 2012; Zhou et al., 2015) in response to basement membranes abnormalities (Abboud Hanna, 2012).

In the present work we tested the hypothesis that *Hgsnat* gene inactivation causes a lysosomal storage disorder in the intraglomerular mesangial cells by studying the kidney pathology in the previously described *Hgsnat* knockout mouse strain (Martins et al., 2015). In mice, *Hgsnat* knockout causes a milder variant of MPSIIIC with prolonged relative life expectancy as compared with that of humans with the disease (Martins et al., 2015), making this model ideal to examine the progressive effects of HGSNAT deficiency and heparan sulfate accumulation in the renal corpuscle, i.e., the region of the nephron that contains the glomerular capillaries. The effect of the disease was assessed by light and electron microscopy and immunocyto-chemistry.

Materials and methods

Animals

Wild type (WT) C57BL/6NCrl mice and C57BL/6NCrl mice with targeted disruption of the *Hgsnat* gene (KO) (7, 11 and 14-months of age; n=3 per each experimental group), were previously described (Martins et al., 2015). All eighteen animals used in this study were maintained on a 12-h dark/light cycle in the animal facility and fed ad libitum. Approval for the animal care and the use in the experiments was granted by the Animal Care and Use Committee of the Ste-Justine Hospital Research Center.

Fixation for morphological and immunogold labeling studies

For morphological studies, animals were anesthetized with sodium pentobarbital and perfused via an intracardiac catheter with 2.5% glutaraldehyde in 0.1 M sodium cacodylate buffer. The left kidneys were removed, the cortex was carefully dissected and trimmed into 2-mm thick cubes with a razor blade. Subsequently, the kidney samples were post-fixed by immersion in 2.5% glutaraldehyde in 0.1 M sodium cacodylate buffer overnight at 4°C. Samples were washed overnight at 4°C in 0.1 M cacodylate washing buffer (pH 7.4). They were then post-fixed with 1% osmium tetroxide and 1.5% potassium ferrocyanide for 2 hours at 4°C, dehydrated and embedded in Epon.

For immunogold labeling experiments, WT and KO mice were anesthetized with pentobarbital. Prior to perfusion, the right kidneys were removed and fixed by immersion in 0.25% glutaraldehyde, 4% para-formaldehyde, and 15 mM lysine at pH 7.4 in 0.1 M phosphate buffer. After 24 hours the cortices were trimmed into small blocks, kept in the same fixative for two hours, and then washed three times in PBS (137 mM NaCl, 2.7 mM KCl, 1.5 mM KH_2PO_4, 6.5 mM Na_2HPO_4, pH 7.4) containing 4% sucrose at 4°C. The tissues were dehydrated in methanol and embedded in LR white resin.

For light microscopy (LM) studies, semithin sections (1 μm thick) were cut, mounted on glass slides, stained with toluidine blue, and visualized with a Leica DMS light microscope. The use of LM allowed us to examine large cortical areas and to select renal corpuscles for electron microscope analysis.

For electron microscopy, ultrathin sections (120 nm thick) were cut with a diamond knife in an ultramicrotome and mounted on 200 mesh copper grids. Staining of the Epon grids was done with uranyl acetate for 5 min, followed by lead citrate for 2 min. The grids were then examined on a Tecnai 12 120 kV transmission electron microscope at the McGill University Facility for Electron Microcopy Research (FEMR). Images were collected with a AMT XR80C CCD camera (Advanced Microscopy Techniques Corp, Woburn, MA) coupled to the microscope.

Immunocytochemistry processing of kidneys

LR White ultrathin sections were mounted on mesh copper grids and placed on a drop of 0.02 M glycine in buffer for 10-15 minutes followed by 5 minutes on a drop of 2% Bovine Casein Ovoalbumin blocking agent (BCO). They were then placed either on a drop of anti-heparan sulfate monoclonal antibody (10E4 epitope, USBiological, 1:15 dilution) or on a drop of anti-prosaposin antibody generated in our lab (Lefrancois et al., 2002) and left to bind for 1 hour. Next, the grids were washed with DPBS buffer (Dulbecco's Phosphate Buffered Saline) for 15-20 minutes and placed on a drop of BCO blocking agent for another 5 minutes. The grids were then placed on a drop of antibody conjugated to gold for 30 minutes. They were then washed with DPBS, 1% glutaraldehyde, and distilled water, dried, and stained with 4% aqueous uranyl acetate for 5 minutes. After another jet wash with distilled water, they were stained with a drop of Reynold's lead for 3 minutes then washed and dried. The grids were analyzed on a Tecnai 12 120kV transmission electron microscope.

Particle count and membrane measurement statistical analysis

To count the number of gold particles bound to podocytes and basement membranes, the Fiji image processing program was used. For this purpose, images of the renal corpuscle taken at 18,500X magnification were used for each group, WT and KO (n=3). For this analysis we used only 11 month old mice since at this age the lysosomal storage was well established in the podocytes of KO animals. The chosen magnification permitted a count of the number of gold particles per unit basement membrane and to determine variations in distribution and concentration of heparan sulfate in WT and KO.

The measurements of basement membrane were carried out using ten electron micrograph images per group (WT and KO) at the ages of 7, 11 and 14 months. The images at 1,900X magnification were randomly selected and the measurements were taken using ImageJ software (Version 1.48, NIH). The values obtained from both particle counting and morphometrical analyses were subjected to the Lilliefors normality test using the software MatLab (MathWorks, Natick, MA, USA). Normality was verified for all samples ($P \geq 0.05$), and means were compared using the student's t-test. Differences between groups were considered statistically significant with $P < 0.05$.

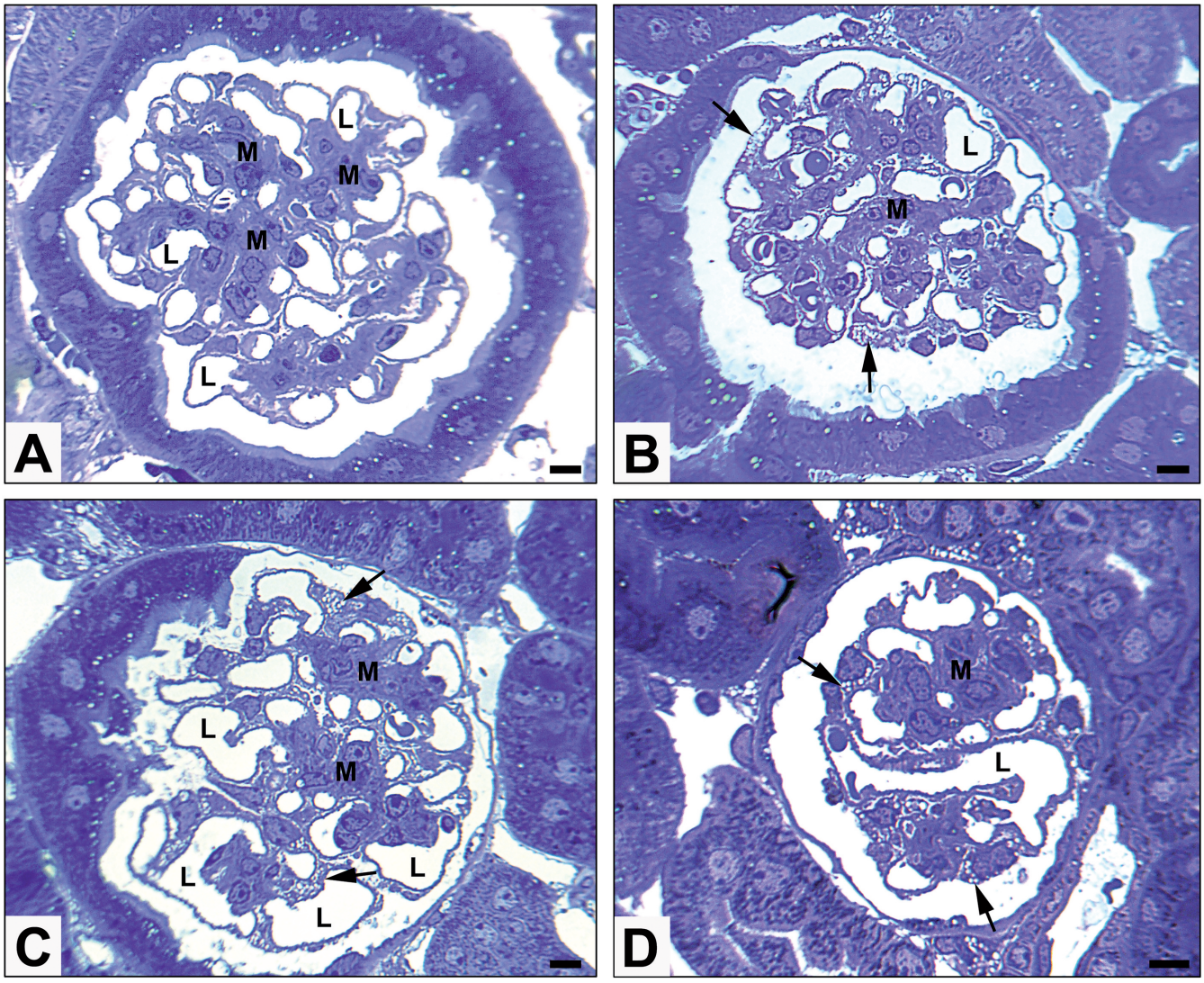

Fig. 1. Light microscope images of renal corpuscles of HGSNAT at 7, 11 and 14 months stained with toluidine blue. **A.** 7 months old WT animals presented no buildup of lysosomes in the intraglomerular cells. **B.** KO animals show a build up of vacuolar structures in intraglomerular cells associated with capillaries (arrows). **C, D.** 11-month and 14-month KO animal sections showing a similar morphological phenotype to the 7-month KO animal. Arrows indicate areas of lysosomal build up. L, lumen of glomerular capillaries; M, mesangial cell. Scale bars: 10 μm.

Results

Light microscopy

Examination of renal corpuscles with the light microscope showed a progressive buildup of vacuoles in intraglomerular cells of KO mice. Under the light microscope, it was unclear which cell type contained the storage. However, their location and morphology corresponded to that of podocytes (Fig. 1A-D). We considered other cell types, such as macrophages, but it was not the case since macrophages were not seen outside the capillary loops. The samples from WT animals did not show any evidence of lysosomal build up and had healthy structures. The differently aged KO animals showed variations in diameter of the renal corpuscle, attributed to the progression of the disease. Generally, the renal corpuscles were smaller in the older animals and exhibited fewer cells, possibly podocytes, most likely due to cell regression (Fig. 1B-D). In addition, a gradual distortion was noted in the shape and size of glomerular capillaries of KO animals (Fig. 1B-D).

Electron microscopy

Observation with the electron microscope allowed us to obtain a clearer image of the affected cells and of their abnormal lysosomes. It also gave us an idea of the general health of the glomerular structures. This diagnosis was based on the visible accumulation of lysosomes, and distortion in intraglomerular basement membrane thickness.

Figure 2A,B illustrate the glomerular appearance in WT and KO kidneys respectively. In both images, it is possible to identify the network of capillaries covered on their luminal side by a fenestrated lining of endothelial cells and on their adventitial side by podocytes with their secondary processes (pedicels) resting on basement membranes enveloping the capillaries. In WT glomeruli, the podocytes and mesangial cells did not show lysosomal build up. In the KO animals, the podocytes contained many vacuoles, typical of a lysosomal storage disorder, but the mesangial cells and endothelial cells were unaffected (Fig. 2A-C). The lysosomes in the podocytes of KO animals appear strained and, in some cases, had burst or were in the process of fusing with

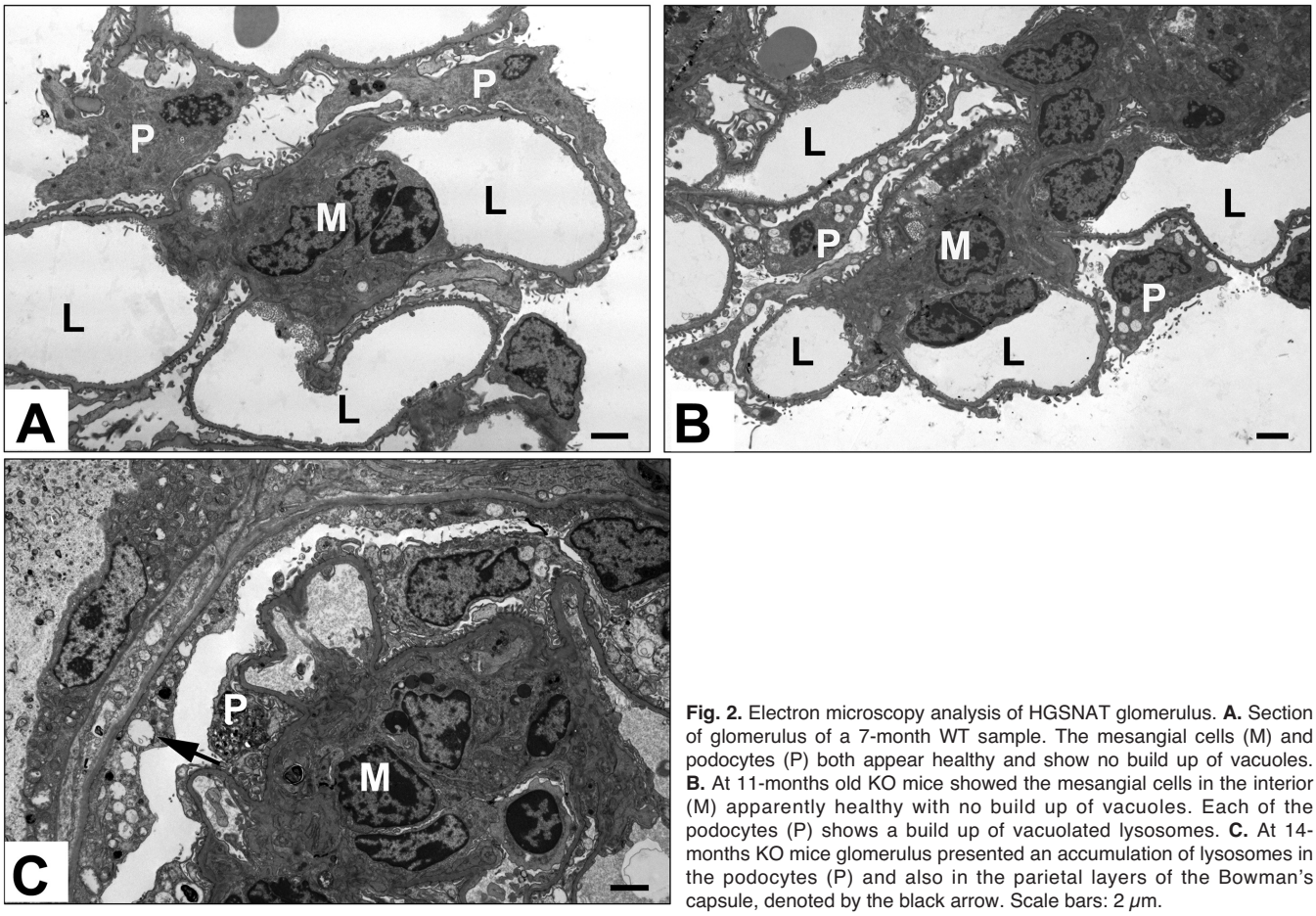

Fig. 2. Electron microscopy analysis of HGSNAT glomerulus. **A.** Section of glomerulus of a 7-month WT sample. The mesangial cells (M) and podocytes (P) both appear healthy and show no build up of vacuoles. **B.** At 11-months old KO mice showed the mesangial cells in the interior (M) apparently healthy with no build up of vacuoles. Each of the podocytes (P) shows a build up of vacuolated lysosomes. **C.** At 14-months KO mice glomerulus presented an accumulation of lysosomes in the podocytes (P) and also in the parietal layers of the Bowman's capsule, denoted by the black arrow. Scale bars: 2 μm.

other lysosomes (Fig. 3B,C). Similarly, the parietal cells of the Bowman's capsule presented an accumulation of lysosomes in the KO mice.

The glomerular basement membrane's thickness showed variations in relation to the age and experimental condition. While in WT kidneys, the membrane had a consistent width around the circumference of the capillaries, in KO kidneys, the glomerular membrane thickness was inconsistent with alternating wide and narrow areas (Fig. 3). For comparison purposes, we measured the thickness of glomerular basement membrane in WT and KO at ages of 7, 11 and 14-months (Fig. 4). A significant decrease was observed in the basal membrane width of the 7 months KO animals (104.9±SE3.7) when compared to WT mice at the same age (143.6±SE2.7). In contrast, KO mice at 14 months presented a significant increase in the width of basal membrane (WT=121.3±SE6.1; KO=194.1±SE8.7). For the KO mice at 11-months, no significant difference between groups was found (WT=124.9±SE6.1; KO=108.9±SE7.6).

Immunogold labeling

Kidneys from 11-month old WT and KO mice were incubated with anti-heparan sulfate antibody followed by a secondary antibody conjugated to gold particles. Gold particles were successfully visualized in the basement width of both WT and KO animals. The particles concentrated on the outer side of the basement

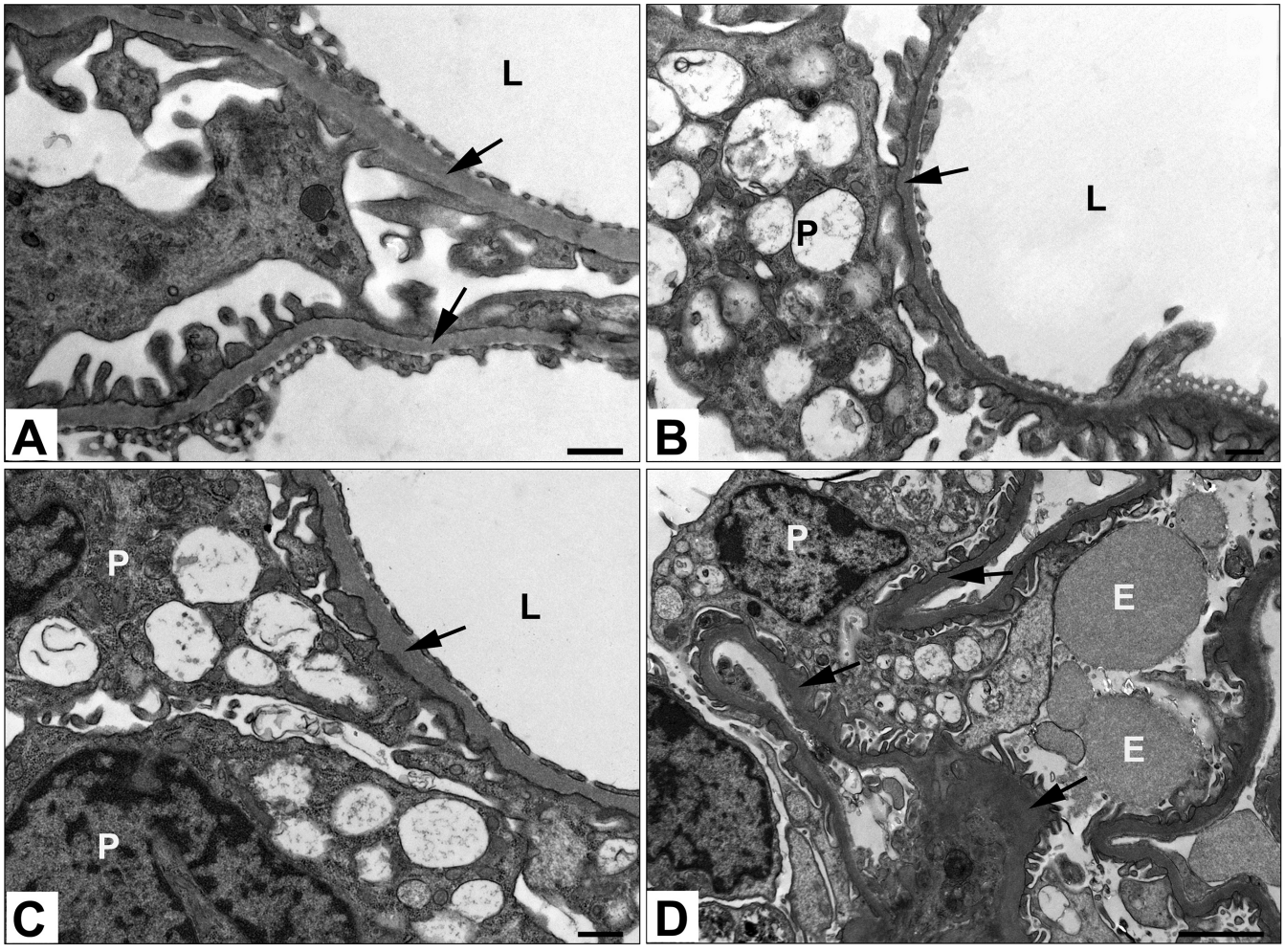

Fig. 3. Analysis of glomerular basal membrane of WT and Hgsnat KO mice **(A)** glomerulus of a 7 month WT animal showing two healthy basement membranes flanking a podocyte. The membranes are of consistent width along their length (arrows). **B.** At 7-months, KO animals presented a build up of lysosomes in the podocyte (P) to the left of the capillary lumen (L). The podocyte is nearly bursting with heparan sulfate-filled lysosomes and the basement membrane appears uneven. **C.** An 11-month KO animal with basement membrane dividing the lumen (L) and podocytes (P). Some lysosomes within the podocyte are broken down or fusing with one another. **D.** A section of glomerulus of a 14-month KO sample. The interior structures appear compressed and the basement membrane varies greatly in width. Arrows point to basement membranes. Scale bars; A-C, 500 nm; D, 2 μm.

membrane, near and around the pedicels (Fig. 5A-C). The localization and quantity of particles suggest a likely route of heparan sulfate transport, from the basement membrane through the pedicels and to the podocytes. While the lysosomes of WT podocytes were rare and did not show heparan sulfate immunogold labelling, they were abundant and moderately labelled in the podocytes of KO kidneys (Fig. 5C). To verify if the podocyte vacuoles were lysosomes, kidneys of KO mice were incubated with anti-prosaposin antibody followed by a secondary antibody conjugated to gold particles. The prosaposin antibody heavily labeled the accumulating vacuoles (Fig, 5D).

Using the anti-heparan sulfate antibody, we estimated the average number of gold particles visualized in the basement membranes of the 11-month WT and KO samples, representing the concentration of heparan sulfate molecules in this structure. Immunogold labeling revealed that there is a three-fold increase in the concentration of heparan sulfate in the basement membrane of knockout mice (4.76±0.59 SEM gold particles per 1000 nm of linear basement membrane) compared to the wild type mice (1.58±0.30 SEM gold particles per 1000 nm of linear basement membrane).

Discussion

The renal corpuscle is 200 μm in diameter and comprises a tuft of capillaries (the glomerulus) and Bowman's capsule (Bulger and Dobyan, 1982). The latter has two epithelial layers. The parietal layer of Bowman's capsule is a simple squamous epithelium and forms the outer limit of the renal corpuscle (Haensly et al., 1982). The inner layer (visceral layer) is formed by highly differentiated cells named podocytes (Mundel and Kriz, 1995). The parietal layer and the podocytes share a common origin, the metanephric mesenchyme

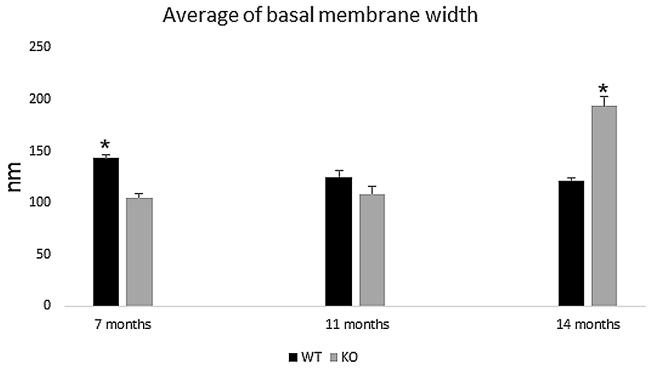

Fig. 4. Morphometric analysis of the glomerular basal membrane of WT and Hgsnat KO mice. Mean width glomerular basement membranes in WT and KO animals at 7, 11 and 14-months (n=3 per group). Values are expressed in nanometers. Asterisks indicate significant differences between 7-months WT and 14-months KO groups (P<0.05).

(Achenbach et al., 2008). The podocyte cells have a cell body from which several primary processes arise, and each primary process gives rise to abundant secondary processes, called pedicels. The pedicels embrace the capillary loops of the glomerulus and interdigitate with pedicels from adjacent podocytes to form filtration slits of 25 nm wide (Bulger and Dobyan, 1982). The glomerular capillaries are fenestrated. Between the endothelial cells of the capillaries of the glomerulus and the pedicels from podocytes, there is a thick basement membrane derived from the fused basal laminas of podocytes and endothelial cells, which represents the filtration barrier separating the blood from the urinary capsular space (Bulger and Dobyan, 1982). Finally, trapped between the loops of capillaries are the intraglomerular mesangial cells. They are considered phagocytic and involved in digestion of extracellular matrix components (Abboud Hanna, 2012). Furthermore, they may be contractile and contribute to controlling blood flow in the glomerulus. They also support the capillary loops in the regions in which podocytes are not in contact with them (Bulger and Dobya, 1982; Abboud Hanna, 2012).

Surprisingly, our results demonstrated lysosomal storage and heparan sulfate accumulation in the podocytes but not in the mesangial cells, suggesting that the podocytes are primarily involved in the degradation of heparan sulfate of glomerular basement membrane. Furthermore, examination of kidney samples from *Hgsnat* knockout animals by light microscopy, electron microscopy, and immunocytochemistry revealed several key findings regarding glomerular basement membranes and progression of lysosomal storage in the podocytes of these mice.

First, we confirmed through immunocytochemistry that accumulation of heparan sulfate is the cause of the observed lysosomal pathology. It was highly visible and abundant in the lysosomes of podocytes and the parietal layer of the Bowman's capsule. The concentration of undigested heparan sulfate is demonstrated by the large number of gold particles visualized in the lysosomal compartment of these cells. Uneven, misshapen basement membranes correlated well with the podocyte defects where heparan sulfate was not properly processed. Interestingly, the increasing concentration of plasma heparan sulfate derived disaccharides and the total concentration of urinary glycosaminoglycans in a large cohort of MPSIII patients showed that they correlate with the disease severity (de Ruijter et al., 2013). This reinforces our interpretation that the hindered processing of heparan sulfate in the Hgsnat knockout may be partially responsible for the poor kidney health of these animals.

The quantitative assessment of immunogold labeling revealed that there is a three-fold increase in the concentration of heparan sulfate in the basement membrane of knockout mice compared to wild type, substantiating the view that there is a widespread problem with heparan sulfate processing in

mucopolysaccharidosis type III kidneys (Ramaswami et al., 1996). The three-fold increase in number of particles in the KO's basement membranes suggests that heparan sulfate is not removed and/or processed effectively, indicative of a malfunction across the entire processing pathway. It is plausible that internalized heparan sulfate accumulates and saturates the lysosomal compartment of podocytes, up to a point where this proteoglycan is no longer removed from the basement membranes. As such, the number of molecules accumulates and the basement membrane becomes increasingly congested and unhealthy. This conclusion is supported by our data on the average basement membrane width of the KO animals. While we cannot explain the drop between the 7-month WT and KO average membrane widths, an increasing trend in the KO membrane thickness is observed in the older KO mice. This accumulation and thickness worsen as the disease progresses to an extent where the increase in width becomes statistically significant. As the diseased animal ages, it is likely that the weakened degradation machinery and congested membrane leads to a decline in effective filtration (Ramaswami et al., 1996).

Renal insufficiency is recognised as the most prevalent clinical sign and the main cause of death in Fabry disease (Del Pino et al., 2018). This condition

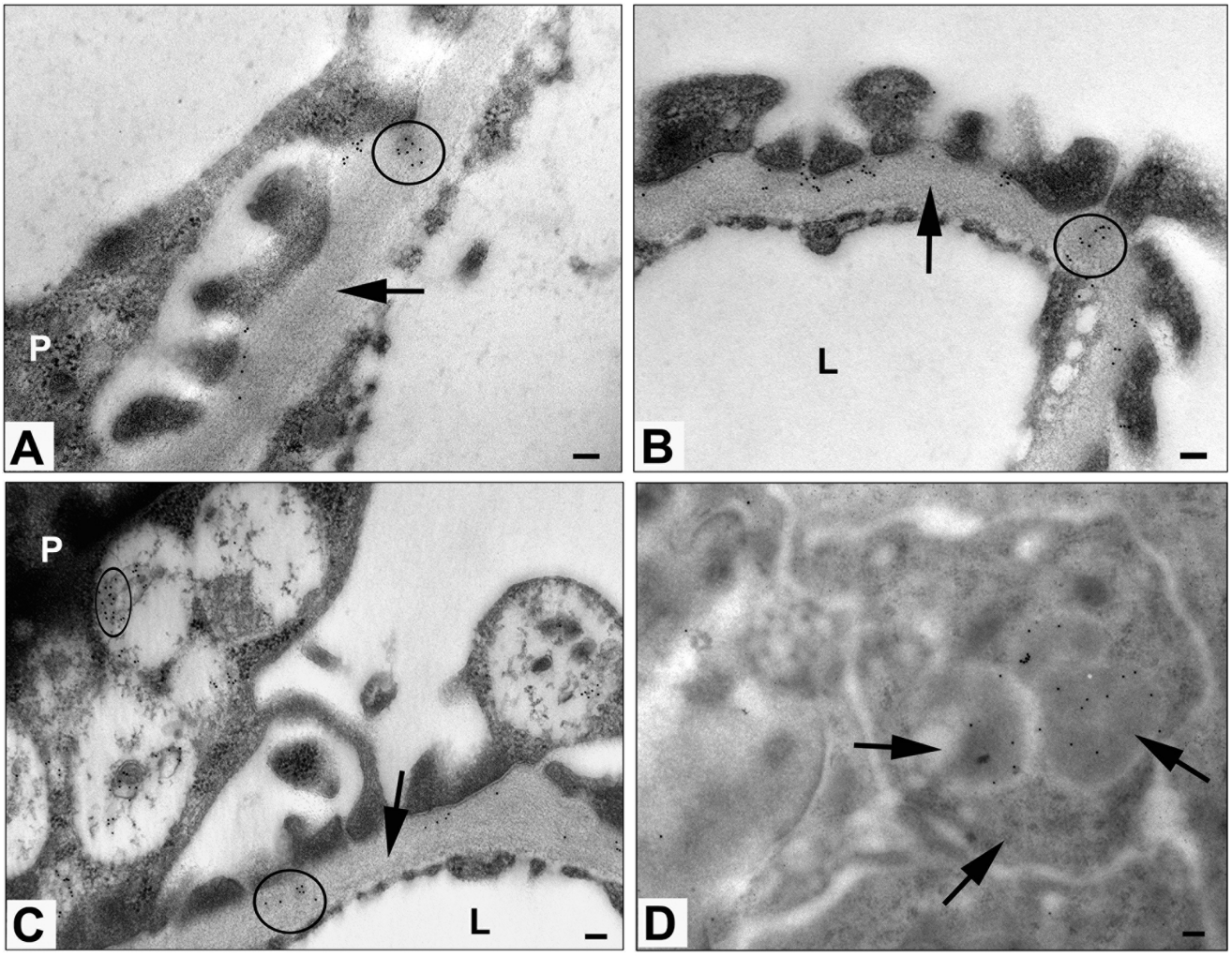

Fig. 5. Immunogold labeling of kidney cortical tissue of 11 month WT and Hgsnat KO mice. **A.** The healthy region of basement membrane (arrow) of a WT animal is lined by fenestrated endothelium and by pedicels on the opposite site. The punctiform structures in the circle represent gold particles bound to heparan sulfate. **B.** At 11-months, KO mice have a higher density of heparan sulfate molecules in basement membrane (arrow and circled gold particles) than WT mice. **C.** The primary process of an 11-month, KO mouse is filled with lysosomes heavily labeled by anti-heparan sulfate antibody (circled gold particles within upper vacuole). The antibody also labeled the basement membrane (arrow and circled gold particles). **D.** The accumulating vacuoles of KO podocytes (arrows) were labeled by the lysosomal marker anti-prosaposin antibody. L, is the lumen of glomerular capillaries and P the primary process of a podocyte. Scale bars: 100 nm.

has also been reported in patients affected by other lysosomal disorders, primarily mannosidosis (Segoloni et al., 1996). Kidney failure has been described in 40% of MPS II (Hunter disease) patients after withdrawal from enzyme replacement therapy (Jurecka et al., 2012) as well as in the feline model of MPS I (Hurler disease) (Cianciolo et al., 2011). Similarly to MPSIIIC, MPSI and MPSII are neurological mucopolysaccharidoses characterized by tissue storage of heparan sulfate.

In Fabry disease, the parallel of proteinuria and lysosomal storage progression in podocytes strongly suggests that the injury of these cells may play a pivotal role in the development of Fabry nephropathy (Najafian et al., 2011; Schiffmann et al., 2009). Although no reports on renal insufficiency in Sanfilippo C patients could be found, it is possible that this condition was unnoticed due to the rapidly progressing neurological disease which is the major burden of the patients leading to dementia and death before their third decade of life (Ruijter et al. 2008). Finally, the most unforeseen conclusion of the experiment is the discovery that processing of heparan sulfate occurs in the podocytes rather than the mesangial cells. The current literature on processing of basement membrane in the kidney is inadequate but suggests that processing of extracellular matrix within the renal corpuscle may occur in intraglomerular mesangial cells (Abboud Hanna, 2012; Zhou et al., 2015). Thus, our observation challenges the current view on the processing of glomerular basement membrane. To our knowledge, this is the first demonstration that undigested heparan sulfate accumulates in lysosomes of the defective podocytes lining the capillaries and in the defective parietal cells of the Bowman capsule. Interestingly, both cells share the same embryological origin. Thus, it is tempting to hypothesize that accumulation of heparan sulfate in the lysosomal compartment was likely the cause of the basement membrane defects. Furthermore, immunogold labeling with the anti-heparan sulfate antibody revealed an accumulation of heparan sulfate around the secondary processes of podocytes both in WT and KO mice suggesting that the pedicels are involved in the removal and/or endocytosis of heparan sulfate. This interpretation is further substantiated by the fact that heparan sulfate concentrates in these areas not only in the knockout mice, but in the WT as well.

In view of our findings documenting severe pathological changes in the kidney of MPSIIIC model mice, an examination of renal function in MPSIIIC patients is deemed necessary.

Acknowledgements. We thank Ms. Jennie Mui, Ms. Lee Ann Monaghan and the Facility for Electron Microscopy Research of McGill University for assistance with microscope operation and tissue preparation. This investigation was supported by an NSERC grant to Carlos R. Morales, and by a Canadian Institutes of Health Research grant and a Canadian Glycomic Network grant to Alexey V. Pshezhetsky.

References

Abboud Hanna E.H. (2012). Mesangial cell biology. Exp. Cell Res. 318, 979-985.

Achenbach J., Mengel M., Tossidou I., Peters I., Park J.-K., Haubitz M., Ehrich J.H., Haller H. and Schiffer M. (2008). Parietal epithelia cells in the urine as a marker of disease activity in glomerular diseases. Nephrol. Dial Transplant. 23, 3138-3145.

Bame K.J. and Rome L.H. (1986). Genetic evidence for transmembrane acetylation by lysosomes. Science 233, 1087-1089.

Bame K.J. (2001). Heparanases: endoglycosidases that degrade heparan sulfate proteoglycans. Glycobiology 11, 91R-98R.

Bartsocas C., Gröbe H., van de Kamp J.J.P., von Figura K., Kresse H., Klein U. and Giesberts M. A.H. (1979). Sanfilippo type C disease: Clinical findings in four patients with a new variant of mucopolysaccharidosis III. Eur. J. Pediatr. 130, 251-258.

Bishop J.R., Schuksz M. and Esko J.D. (2007). Heparan sulphate proteoglycans fine-tune mammalian physiology. Nature 446, 1030-1037.

Bulger R.E. and Dobyan D.C. (1982). Recent advances in renal morphology. Annu. Rev. Physiol. 44, 147-179.

Cianciolo R.E., Rhodes J.L., Haskins M.E., Clubb F.J. and Lees G.E. (2011). Renal failure associated with mucopolysaccharidosis type I in a cat from a MPS I research colony. Comp. Med. 61, 441-444.

de Ruijter J., Ijlst L., Kulik W., van Lenthe H., Wagemans T., van Vlies N. and Wijburg F.A. (2013). Heparan sulfate derived disaccharides in plasma and total urinary excretion of glycosaminoglycans correlate with disease severity in Sanfilippo disease. J. Inherit. Metab. Dis. 36, 271-279.

Del Pino M., Andrés A., Bernabéu A.Á., de Juan-Rivera J., Fernández E., de Dios García Díaz J., Hernández D., Luño J., Fernández I.M., Paniagua J., Posada de la Paz M., Rodríguez-Pérez J.C., Santamaría R., Torra R., Ambros J.T., Vidau P. and Torregrosa J.V. (2018). Fabry Nephropathy: An Evidence-Based Narrative Review. Kidney Blood Press Res. 43, 406-421.

Feldhammer M., Durand S., Mrázová L., Boucher R-M., Laframboise R., Steinfeld R., Wraith J.E., Michelakakis H., van Diggelen O.P., Hřebíček M., Kmoch, S. and Pshezhetsky A.V. (2009). Sanfilippo syndrome type C: mutation spectrum in the heparan sulfate acetyl-CoA: alpha-glucosaminide N-acetyltransferase (HGSNAT) gene. Hum. Mutat. 30, 918-925.

Haensly W.E., Granger H.J., Morris A.C. and Cioffe C. (1982). Proximal-tubule-like epithelium in Bowman's capsule in spontaneously hypertensive rats. Am. J. Pathol. 107, 92-97.

Hrebícek M., Mrázová L., Seyrantepe V., Durand S., Roslin N.M., Nosková L., Hartmannová H., Ivánek R., Cízkova A., Poupetová H., Sikora J., Urinovská J., Stranecký V., Zeman J., Lepage P., Roquis D., Verner A., Ausseil J., Beesley C.E., Maire I., Poorthuis B.J. van de Kamp J., van Diggelen O.P., Wevers R.A., Hudson T.J., Fujiwara T.M., Majewski J., Morgan K., Kmoch S. and Pshezhetsky A.V. (2006) Mutations in TMEM76* cause mucopolysaccharidosis IIIC (Sanfilippo C syndrome). Am. J. Hum. Genet. 79, 807-819.

Jurecka A., Żuberuber Z., Opoka-Winiarska V., Węgrzyn G. and Tylki-Szymańska A. (2012). Effect of rapid cessation of enzyme replacement therapy: a report of 5 cases and a review of the literature. Mol. Genet. Metab. 107, 508-512.

Lefrancois S., May T., Knight C., Bourbeau D. and Morales C.R. (2002). The lysosomal transport of prosaposin requires the conditional interaction of its highly conserved d domain with sphingomyelin. J.

Biol. Chem. 277(19), 17188-17199.

Martins C., Hůlková H., Dridi L., Dormoy-Raclet V., Grigoryeva L., Choi Y., Martins C., Langford-Smith A., Wilkinson F.L., Ohmi K., DiCristo G., Hamel E., Ausseil J., Cheillan D., Moreau A., Svobodová E., Hájková Z., Tesařová M., Hansíková H., Bigger B.W., Hrebícek M. and Pshezhetsky A.V. (2015). Neuroinflammation, mitochondrial defects and neurodegeneration in mucopolysaccharidosis III type C mouse model. Brain 138, 336-355.

Miner J.H. (2012). The Glomerular Basement Membrane. Exp. Cell Res. 318, 973-978.

Mundel P. and Kriz W. (1995). Structure and function of podocytes: an update. Anat. Embryol. 192, 385-397.

Najafian B., Svarstad E., Bostad L., Gubler M.C., Tøndel C., Whitley C. and Mauer M. (2011). Progressive podocyte injury and globotriaosylceramide (GL-3) accumulation in young patients with Fabry disease. Kidney Int. 79, 663-670.

Ramaswami U., Van 'tHoff W., Clayton P. and Vellodi A. (1996). Sanfilippo disease (mucopolysaccharidosis type III) presenting as transient renal tubular dysfunction. J. Inherit. Metab. Dis. 19, 87-88.

Ruijter G.J., Valstar M.J., van de Kamp J.M., van der Helm R.M., Durand S., van Diggelen O.P., Wevers R.A., Poorthuis B.J., Pshezhetsky A.V. and Wijburg F.A. (2008). Clinical and genetic spectrum of Sanfilippo type C (MPS IIIC) disease in The Netherlands. Mol. Genet. Metab. 93, 104-111.

Schiffmann R., Warnock D.G., Banikazemi M., Bultas J., Linthorst G.E., Packman S., Sorensen S.A., Wilcox W.R. and Desnick R.J. (2009). Fabry disease: progression of nephropathy, and prevalence of cardiac and cerebrovascular events before enzyme replacement therapy. Nephrol. Dial. Transplant. 24, 2102-2111.

Segoloni G.P., Colla L., Messina M. and Stratta P. (1996). Renal transplantation in a case of mannosidosis. Transplantation. 61, 1654-1655.

Valstar M.J., Ruijter G.J.G., van Diggelen O.P., Poorthuis B.J. and Wijburg F.A. (2008). Sanfilippo syndrome: A mini-review. J. Inherit. Metab. Dis. 31, 240-252.

White K.E. (2012). Research into the structure of the kidney glomerulus – making it count. Micron 43, 1001-1009.

Wilson H.M. and Stewart K.N. (2012). Human cell culture protocols. 3rd ed. Mitry, R.R. and Hughes, R.D. (eds). Humana Press. Totowa, NJ. pp 187-201.

Zhou X., Workeneh B., Hu Z. and Li R. (2015). Effect of immunosuppression on the human mesangial cell cycle. Mol. Med. Rep. 11, 910-916.

Accepted June 3, 2019